

Lingfeng Yang

Key Laboratory of Education Ministry for Modern
Design and Rotor-Bearing System,
School of Mechanical Engineering,
Xi'an Jiaotong University,
Xi'an, Shaanxi 710049, China
e-mail: leaf_xjtu@stu.xjtu.edu.cn

Tonghai Wu¹

Key Laboratory of Education Ministry for Modern
Design and Rotor-Bearing System,
School of Mechanical Engineering,
Xi'an Jiaotong University,
Xi'an, Shaanxi 710049, China
e-mail: wt-h@163.com

Kunpeng Wang

Key Laboratory of Education Ministry for Modern
Design and Rotor-Bearing System,
School of Mechanical Engineering,
Xi'an Jiaotong University,
Xi'an, Shaanxi 710049, China
e-mail: moyuansuishang@163.com

Hongkun Wu

School of Mechanical and Manufacturing
Engineering,
The University of New South Wales,
Sydney, NSW 2052, Australia
e-mail: hongkun.wu@unsw.edu.au

Ngaiming Kwok

School of Mechanical and Manufacturing
Engineering,
The University of New South Wales,
Sydney, NSW 2052, Australia
e-mail: nmkwok@unsw.edu.au

Optimum Color and Contrast Enhancement for Online Ferrography Image Restoration

Online ferrography, because of its nondestructive and real-time capability, has been increasingly applied in monitoring machine wear states. However, online ferrography images are usually degraded as a result of undesirable image acquisition conditions, which eventually lead to inaccurate identifications. A restoration method focusing on color correction and contrast enhancement is developed to provide high-quality images for subsequent processing. Based on the formation of a degraded image, a model describing the degradation is constructed. Then, cost functions consisting of colorfulness, contrast, and information loss are formulated. An optimal restored image is obtained by minimizing the cost functions, in which parameters are properly determined using the Lagrange multiplier. Experiments are carried out on a collection of online ferrography images, and results show that the proposed method can effectively improve the image both qualitatively and quantitatively. [DOI: 10.1115/1.4044049]

Keywords: online ferrography, image formation model, image restoration, color correction, contrast enhancement

1 Introduction

As a nondestructive evaluation technique, wear debris analysis has been proven to be effective to reveal wear mechanism and give an early warning of components failure [1,2]. Machine wear states are estimated by inspecting the features of the wear debris contained in lubricant, providing references for the condition-based maintenance system to determine the scheduling of corrective maintenance. Thus, catastrophic breakdowns due to wear failure are avoided [3].

Wear debris analysis has been widely used in experimental researches and industrial applications [4,5]. Among the techniques, images of wear debris can be obtained by ferrography. From these images, more accurate features including concentration, size, wear rate, and composition of debris can provide more reliable indications about the machine condition [6]. On the contrary, other methods only represent features of wear debris indirectly. For example, the technique based on magnetic induction takes the number of voltage pulses as the number of wear debris [7]. However, a complete cycle of traditional ferrography operation is time consuming and expensive. Moreover, the entire process, especially the analysis, relies on manual tasks. To make ferrography analysis automatic and real time, the online visual ferrography system was developed [8]. This system uses an electromagnetic

field to periodically attract wear debris and then captures images using a camera. Finally, image processing and pattern recognition techniques are utilized to infer wear states automatically [9–11].

Since the environment in which the online ferrography system works is inferior to that of conventional methods, such as being affected by scattered light from oil and wear debris accumulation, the contrast of the captured image decreases and color cast occurs. Therefore, it becomes difficult to identify wear debris from morphology and color. To obtain accurate results, preprocessing operations are required.

For video-based ferrography, motion blur is the dominating degradation, and Wiener filtering [12] and detailed point spread function estimation [13] were conducted to restore degradations. An adaptive enhancement in which the gain factor changes with the distance to the image center was applied to the restoration of out of focus [14].

Different from the degradations mentioned earlier, the cause of image degradations considered in this work is similar to that in aerial and underwater images. Over the past decades, various methods have been proposed to remove the degradation impacts and improve the image quality. Methods including histogram equalization (HE), unsharp masking filtering (UMF), and homomorphic filtering are common contrast enhancement approaches [15–17]. Histogram equalization expands the range of pixel intensity, but regions with nonuniform illumination are enhanced at the same time. With the consideration of color correction, Retinex-based methods, for instance, automatic color equalization (ACE), are widely applied [18,19]. Although automatic color equalization

¹Corresponding author.

Manuscript received March 20, 2019; final manuscript received June 12, 2019; published online July 3, 2019. Assoc. Editor: K. Elliott Cramer.

has shown promising results in color constancy, nonuniform illumination becomes obvious due to dynamic data stretching.

When considering the cause of image degradation, the impact of haze can be well removed by the dark channel prior method [20]. However, this method does not work when there are high-intensity objects in images. Furthermore, the method relying on the assumption that the transmission and surface shading are locally uncorrelated was developed [21]. However, it cannot handle heavily hazy images well and may fail in cases where the assumption is not valid. In addition, approaches based on light attenuations in different wavelengths were proposed to restore images, especially under macroscopic conditions [22,23]. In the case of microscopic images considered here, attenuations are extremely small. Other than that, compared with haze-free images, degraded images have lower contrast. There had been attempts to optimally restore image by maximizing its contrast value without any intend to recover their original color [24–26].

In this work, instead of blind restoration, an algorithm based on a model describing the cause of degradation is developed. According to the comparison between online ferrography images and offline images captured by the conventional method, priors are proposed to formulate cost functions and constraints. Both contrast enhancement and color correction are considered, because color is crucial for the identification of the wear debris composition. Images are restored by minimizing the cost functions, where optimal parameters are obtained using the Lagrange multiplier.

The rest of the paper is organized as follows: In Sec. 2, a brief introduction is given to online ferrography and image degradation. The developed image restoration approach is described in detail in Sec. 3. Section 4 reports experiments carried out to verify the performance of the proposed method. Results are evaluated and discussed. Finally, a conclusion is drawn in Sec. 5.

2 Brief Introduction of Online Ferrography and Image Degradation

A complete cycle of traditional ferrography operation primarily consists of oil sampling, slide making, image capturing, and debris identification. These four steps are manually carried out at different times and in different places. To make it automatic, online ferrography is essentially a technique integrating all those procedures and allows for a short operation cycle.

2.1 Online Ferrography. The principle of online ferrography is illustrated in Fig. 1. A stream of metallic debris is produced from machine component contact and fatigue and then delivered by a pump to a sensor installed on the oil returning pipe. The sensor is made up of three parts: electromagnet, micro-flow channel, and camera. Wear debris carried in the lubricant are deposited by the

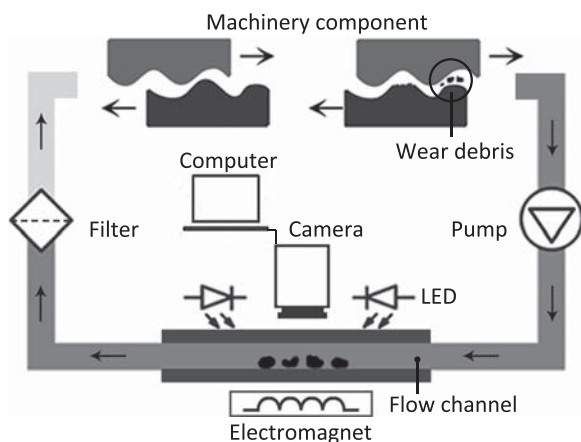


Fig. 1 Schematic diagram of online ferrography process

magnetic field when going through the flow channel, and images are captured by the camera. The images are stored in the 8-bit BMP red-green-blue color format, and the size is 640×480 pixels width by height.

2.2 Image Degradation. A typical online ferrography image is shown in Fig. 2(a). From this image, gray level features can be extracted for wear debris separation [27], and color features are useful in the classification of wear debris [28]. However, the image has both poor contrast and low colorfulness, which have significant impacts on subsequent processes.

An offline image is shown in Fig. 2(b). This image has a higher quality than the image taken online. It is not difficult to find that different capturing environments lead to different image qualities. Online ferrography works in an environment with lubricant contamination and nonuniform illumination. The poor performance of online image is mainly caused by the following factors:

- (1) The properties of the oil change over time, such as refractive index. Moreover, lights are scattered by the microscopic particles in the lubricant, especially contaminated lubricant.
- (2) The sensor is made of metal, and the inner surface around the camera reflects light.
- (3) Wear debris as microscopic particles also produce light scattering.

These factors are major causes of challenges in online ferrography. Thus, preprocessing is very necessary before extracting information from online images. In this work, a restoration method is developed to remove the influence of scattered light and improve the image performance in both contrast and color.

3 Proposed Method

A block diagram of the image restoration process is shown in Fig. 3. The process is carried out in three steps. First, a model is constructed to describe the degradation, and the image is divided into

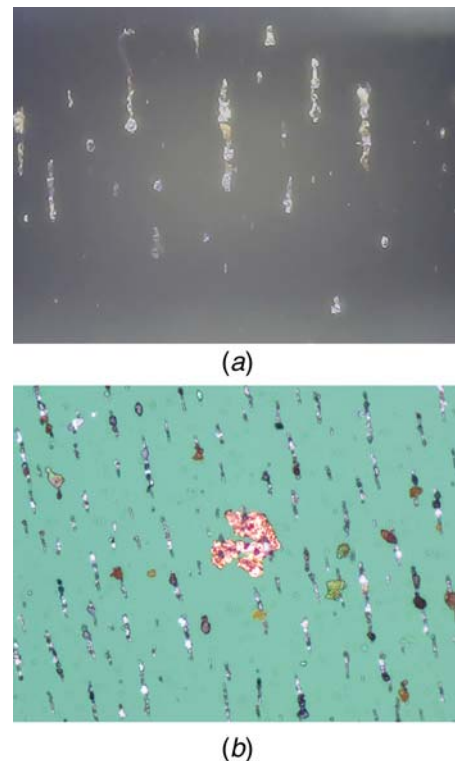


Fig. 2 Ferrography images: (a) online image and (b) offline image

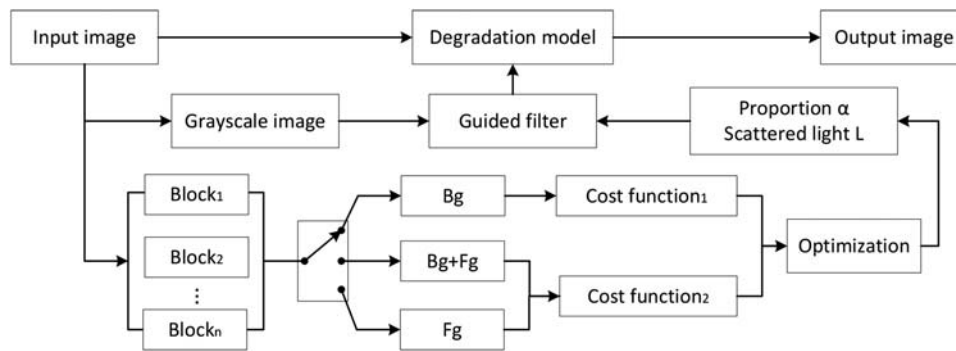


Fig. 3 Block diagram of online ferrography image restoration process

blocks. Then, combined with priors, a cost function is formulated in each image block. Finally, optimal parameters are obtained by minimizing the cost function with Lagrange multiplier. Details are presented in the following sections.

3.1 Degradation Model Construction. Figure 4 illustrates the process of image capture. In fact, lights entering the camera come from two sources. One is the reflection from wear debris as shown by the solid lines, and the other shown by the dotted lines is the scattered light from other objects other than wear debris, for instance, glass and oil. Obviously, the former should be retained, while the latter needs to be removed. The degradation process is shown in Fig. 5. The original image can be obtained by removing the influence of scattered light.

Assume that I represents the observed image that is captured by the camera, and R represents the original image that is an idealized reconstruction. The degradation process can be described as follows:

$$I^c(u, v) = R^c(u, v)\alpha(u, v) + L^c(u, v)[1 - \alpha(u, v)] \quad (1)$$

where $c \in \{r, g, b\}$ represents one of the color channels, (u, v) is the pixel coordinate, $u = 1, 2, \dots, U$, $v = 1, 2, \dots, V$, and U and V are image width and height, respectively. L represents the scattered light, and α represents the proportion of the original image. All variables range from 0 to 1. In practice, the original image and its proportion in the observed image are not known. To restore the original image, R , L , and α have to be obtained in advance.

3.2 Priors Proposal. Although L and α vary over pixels, the differences are small within an image block. Thus, these variables are assumed to be constant. According to Eq. (1), the block in the original image can be obtained by

$$R^c(u, v) = \frac{I^c(u, v) - L^c}{\alpha} + L^c \quad (2)$$

where $(u, v) \in \Omega_i$, Ω_i represents a block in the image. Equation (2) is an indeterminate equation, and the restored results change with L

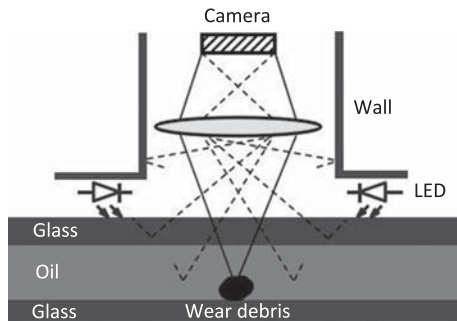


Fig. 4 Image capture process

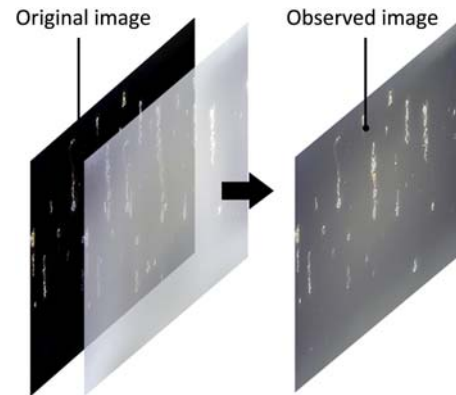


Fig. 5 Image degradation formation

and α in each block. Additional information is required to solve this problem. However, only a single image is available. As mentioned in Sec. 2, it is the environment that degrades the image. Thus, offline images can be regarded as ground truth, while online images are taken as degraded images. Statistical priors about color and contrast are proposed from the comparison between a collection of these images. In addition, a prior about the image background is found by tracking the illumination.

First, as shown in Fig. 2, the offline image has a better appearance in both contrast and color than the online image. Quantitative metrics should be chosen to describe the differences. To this end, 50 online images and 50 offline images are collected for quantitative comparison. Since the image backgrounds are different, only the wear debris pixels are considered. Statistical results from these images against color performance criteria, colorfulness and hue standard deviation, are depicted in box plots in Fig. 6. Here, colorfulness is defined as follows [29]:

$$C = \sigma_{rgyb} + 0.3 \cdot \mu_{rgyb} \quad (3)$$

where

$$\sigma_{rgyb} = \sqrt{\sigma_{rg}^2 + \sigma_{yb}^2} \quad (4)$$

$$\mu_{rgyb} = \sqrt{\mu_{rg}^2 + \mu_{yb}^2} \quad (5)$$

where σ_{rg} and μ_{rg} are the standard deviation and mean value of Δrg , respectively. Similarly, σ_{yb} and μ_{yb} are the standard deviation and mean value of Δyb , respectively, where

$$\Delta rg = r - g \quad (6)$$

$$\Delta yb = 0.5 \cdot (r + g) - b \quad (7)$$

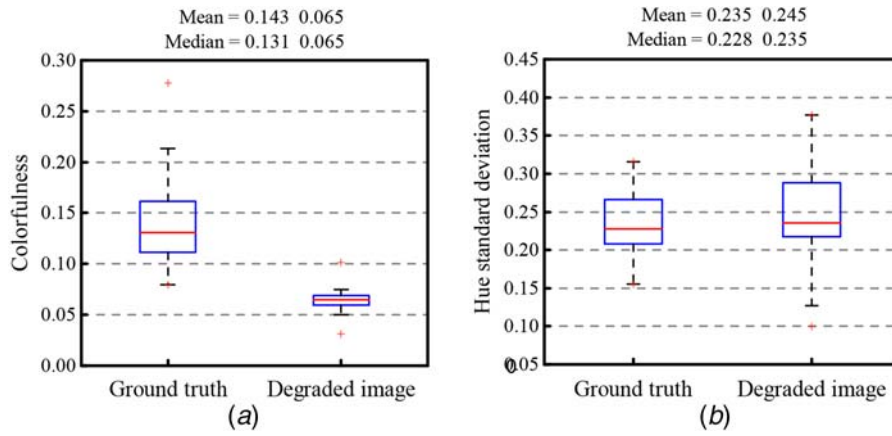


Fig. 6 Statistical results of color criteria: (a) colorfulness and (b) hue standard deviation

The hue standard deviation H is defined as follows:

$$H = \sqrt{\frac{\sum_{i=1}^n (h_i - \bar{h})^2}{n}} \quad (8)$$

where h_i represents the hue value of each pixel in the HSV color space, \bar{h} represents the mean value, and n is the number of pixels.

In Fig. 6(a), degraded images have an average colorfulness of 0.065, which is much lower than 0.143 of the ground truth. From Fig. 6(b), the two groups have almost the same level in the hue standard deviation, i.e., 0.235 and 0.245, respectively. Therefore, colorfulness is an effective criterion to distinguish degraded images from ground truths. The colorfulness of degraded image has a significant degradation due to environment impact, and this criterion should return to the ground truth average after restoration.

With respect to contrast metric, entropy and intensity standard deviation (ISD) are collected and shown in box plots, see Fig. 7. Entropy is given by the following equation:

$$E = - \sum_{i=0}^{255} p_i \log_2(p_i) \quad (9)$$

where p_i is the probability of the occurrence of the i th magnitude.

The intensity standard deviation is defined as follows:

$$T = \sqrt{\frac{\sum_{i=1}^n (s_i - \bar{s})^2}{n}} \quad (10)$$

where s_i represents the intensity of each pixel in grayscale image, \bar{s} represents the mean intensity value, and n is the number of pixels. The grayscale image is given by the following equation:

$$s = 0.299r + 0.587g + 0.114b \quad (11)$$

As shown in Fig. 7, with the influence of the scattered light, intensity standard deviation shows a sharp drop while entropy keeps general steady. Thus, intensity standard deviation is here taken to quantify the contrast, and its value of the restored image should go up to about 0.274.

Apart from the statistical priors about color and contrast illustrated before, there is another prior about image background. As shown in Fig. 8, it can be found that the light goes through the gap between wear debris and transmits through the glass surface with only a very small portion reflected. Thus, these areas should be close to black in the original image. It can be expressed as follows:

$$R_b^c(u, v) \rightarrow 0 \quad (12)$$

where b represents the areas without wear debris.

Combined with Eq. (2), we have

$$I_b^c(u, v) = L^c(1 - \alpha) \quad (13)$$

However, Eq. (13) has no solution unless $I_b^c(u, v)$ is constant within a $m \times m$ block. Thus, it is approximated as follows:

$$\bar{I}_b^c = L^c(1 - \alpha) \quad (14)$$

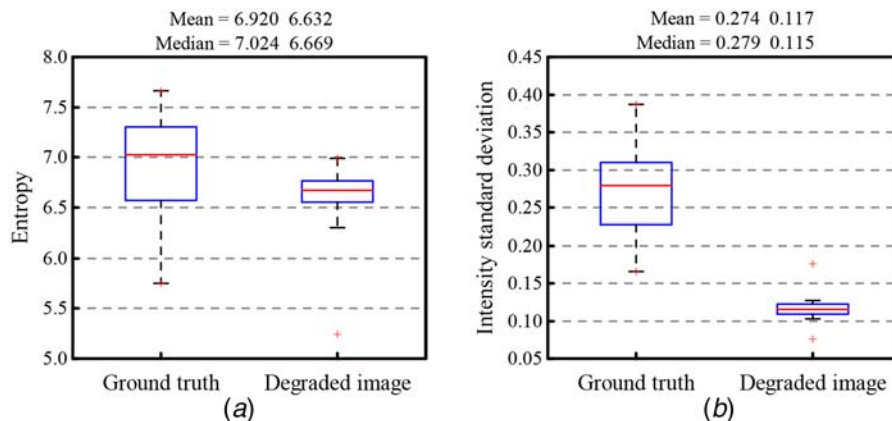


Fig. 7 Statistical results of contrast criteria: (a) entropy and (b) intensity standard deviation

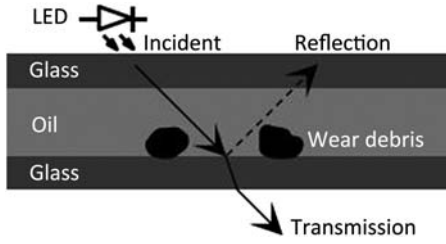


Fig. 8 Illumination tracking

where

$$\bar{I}_b^c = \frac{\sum_{i=1}^m \sum_{j=1}^m I_b^c(i, j)}{m^2} \quad (15)$$

3.3 Cost Function Formulation. In a ferrography image, wear debris is regarded as foreground (Fg), and the others are background (Bg). The image blocks can be classified into three groups: Bg only, Bg and Fg, and Fg only.

For the first group, the restored contrast should be minimized for nonuniform background removal, and information loss should also be minimized during the restoration, see Eq. (2). With respect to the two objectives, a cost function concerning contrast and information loss is defined as follows:

$$f_1 = \omega_1 \cdot T(\alpha, L^c) + \omega_2 \cdot P(\alpha, L^c) \quad (16)$$

where T represents the intensity standard deviation of a restored image block. Combined with Eqs. (2), (10), and (11), T varies with L and α . Since Eq. (2) is actually a linear transformation function from input $I^c(u, v)$ to output $R^c(u, v)$ as shown in Fig. 9, the input higher than b or lower than a leads to information loss. P represents information loss, and it is defined in Eq. (17).

$$P(\alpha, L^c) = \sum_{c \in r, g, b} \left\{ \sum_{i=0}^a \left[\left(\frac{i^c/255 - L^c}{\alpha} + L^c \right)^2 z_i^c \right] + \sum_b^{255} \left[\left(\frac{i^c/255 - L^c}{\alpha} + L^c - 1 \right)^2 z_i^c \right] \right\} \quad (17)$$

where z_i^c represents the number of the occurrence of the i th magnitude in color channel c , a is the intensity corresponding to output 0, and b is the intensity corresponding to output 255 that is further normalized to 1. Since ω_1 and ω_2 are weighting parameters and

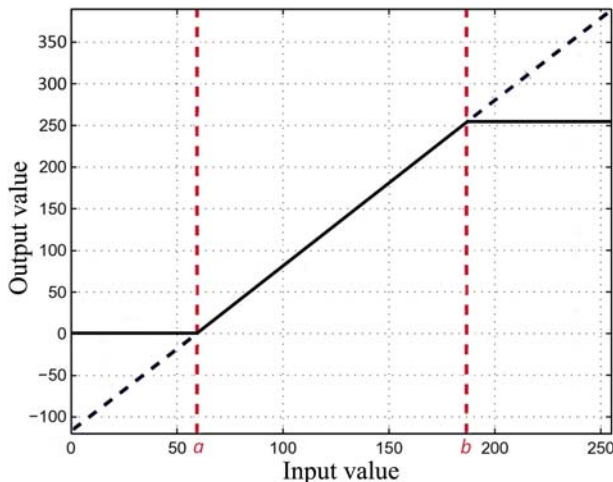


Fig. 9 An example of the transformation function

image contrast is more important than information loss, thus, we have

$$0 < \omega_2 \leq \omega_1 < 1 \quad (18)$$

$$\omega_1 + \omega_2 = 1 \quad (19)$$

For the other two groups, a cost function consisting of contrast, color, and information loss is formulated to measure the differences between the restored images and ground truth. To remove the environmental influence, the differences should be minimized. Note that only foreground pixels are considered in the cost function, and background pixels are used as constraints in Eq. (13) if they exist. Based on the priors mentioned before, the cost function is defined as follows:

$$f_2 = \eta_1 \cdot [C(\alpha, L^c) - 0.143]^2 + \eta_2 \cdot [T(\alpha, L^c) - 0.274]^2 + \eta_3 \cdot P(\alpha, L^c) \quad (20)$$

where C represents colorfulness of a restored block and η_1 , and η_2 , η_3 are weighting parameters. Since color extraction is the unique feature that makes ferrography more advantageous than other techniques, thus, we have

$$0 < \eta_3 \leq \eta_2 \leq \eta_1 < 1 \quad (21)$$

$$\eta_1 + \eta_2 + \eta_3 = 1 \quad (22)$$

3.4 Parameters Optimization. Parameters in cost functions significantly affect the restored results, and they should be optimized to recover more accurate wear debris information. The aim is to minimize the cost functions within a series of constraints. In this work, Lagrange multiplier is employed to obtain the optimal results.

The Lagrangian is given by:

$$\mathcal{L}(\mathbf{x}, \lambda_i, \mu_i) = f(\mathbf{x}) + \sum_{i=1}^M \lambda_i g_i(\mathbf{x}) + \sum_{j=1}^N \mu_j k_j(\mathbf{x}) \quad (23)$$

where \mathbf{x} represents unknown parameters and $f(\mathbf{x})$ is the function to be minimized, that is, the cost function in this work. g_i represent equality constraints, and k_i represent inequality constraints. λ_i and μ_i are Lagrange multipliers. M and N are the numbers of equality constraints and inequality constraints, respectively.

For a block belonging to the first group, the parameters are $\mathbf{x} = [\alpha, L^c, \omega_1, \omega_2]^T$. Equality constraints are derived from Eqs. (14) and (19) as follows:

$$\begin{cases} g_1 = \bar{I}_b^c - L^c(1 - \alpha) = 0 \\ g_2 = \omega_1 + \omega_2 - 1 = 0 \end{cases} \quad (24)$$

Inequality constraints from Eq. (18) and feasible ranges are as follows:

$$\begin{cases} k_1 = \omega_1 - 1 \leq 0 \\ k_2 = \omega_2 - \omega_1 \leq 0 \\ k_3 = -\omega_2 \leq 0 \\ k_4 = L^c \leq 1 \\ k_5 = -L^c \leq 0 \\ k_6 = \alpha \leq 1 \\ k_7 = -\alpha \leq 0 \end{cases} \quad (25)$$

For blocks with foreground and background pixels, the parameters are $\mathbf{x} = [\alpha, L^c, \eta_1, \eta_2, \eta_3]^T$. Equality constraints deriving from Eqs. (14) and (22) are as follows:

$$\begin{cases} g_1 = \bar{I}_b^c - L^c(1 - \alpha) = 0 \\ g_2 = \eta_1 + \eta_2 + \eta_3 - 1 = 0 \end{cases} \quad (26)$$

Inequality constraints from Eq. (21) and feasible ranges are as follows:

$$\begin{cases} k_1 = \eta_1 - 1 \leq 0 \\ k_2 = \eta_2 - \eta_1 \leq 0 \\ k_3 = \eta_3 - \eta_2 \leq 0 \\ k_4 = -\eta_3 \leq 0 \\ k_5 = L^c \leq 1 \\ k_6 = -L^c \leq 0 \\ k_7 = \alpha \leq 1 \\ k_8 = -\alpha \leq 0 \end{cases} \quad (27)$$

For blocks with only foreground pixels, their processing is the same with pixels in the second group except for equality constraints. The equality constraint is as follows:

$$g_1 = \eta_1 + \eta_2 + \eta_3 - 1 = 0 \quad (28)$$

The optimization problem with constraints is converted to unconstrained problem by the Lagrange multiplier. Optimal parameters are obtained by solving the first-order derivative under the Karush–Kuhn–Tucker conditions. It can be expressed as follows:

$$\begin{cases} \nabla_{\mathbf{x}} \mathcal{L}(\mathbf{x}, \lambda_i, \mu_i) = 0 \\ g_i = 0 \\ k_j \leq 0 \\ \mu_j \geq 0 \\ \mu_i k_j = 0 \end{cases} \quad (29)$$

3.5 Parameters Refinement. Although optimal L and α are calculated by the Lagrange multiplier approach in each block, they should be further refined to the pixel bases. Otherwise there will be significant changes at the boundaries between the blocks in the resultant image, as shown in Fig. 10(d).

As an edge-preserving smoothing method, the guided filter has been applied in transmission refinement of the image haze removal. This technique computes the filtering output by

considering the content of a guidance image, and it is defined as follows [30]:

$$q_i = \bar{a}_i G_i + \bar{b}_i \quad (30)$$

where q represents the output and G represents the guided image, and

$$\bar{a}_i = \frac{1}{|w|} \sum_{k \in w_k} a_k \quad (31)$$

$$\bar{b}_i = \frac{1}{|w|} \sum_{k \in w_k} b_k \quad (32)$$

where $|w|$ is the number of pixels in a window w_k and a_k and b_k are linear coefficients assumed to be constant in w_k ,

$$a_k = \frac{1}{|w|} \frac{\sum_{i \in w_k} G_i p_i - \mu_k \bar{p}_k}{\sigma_k^2 + \varepsilon} \quad (33)$$

$$b_k = \bar{p}_k - a_k \mu_k \quad (34)$$

where μ_k and σ_k^2 are the mean and variance of G in w_k , respectively, p represents the input, \bar{p}_k is the mean value of p in w_k , and ε is defined as a small number. In this work, the grayscale image of the observed image I is used as a guided image, and L and α are taken as inputs. Results are shown in Fig. 11. After the refinement, the restored image is finally obtained according to Eq. (1).

4 Experimental Results

A collection of 50 test images captured from the online ferrography device is used to evaluate the performance of the proposed restoration method. All images are of 640×480 pixels in the BMP format. The block size is 32×32 pixels. For convenience, the optimum color and contrast enhancement method proposed in this work is abbreviated as OCCE, and related restoration methods are

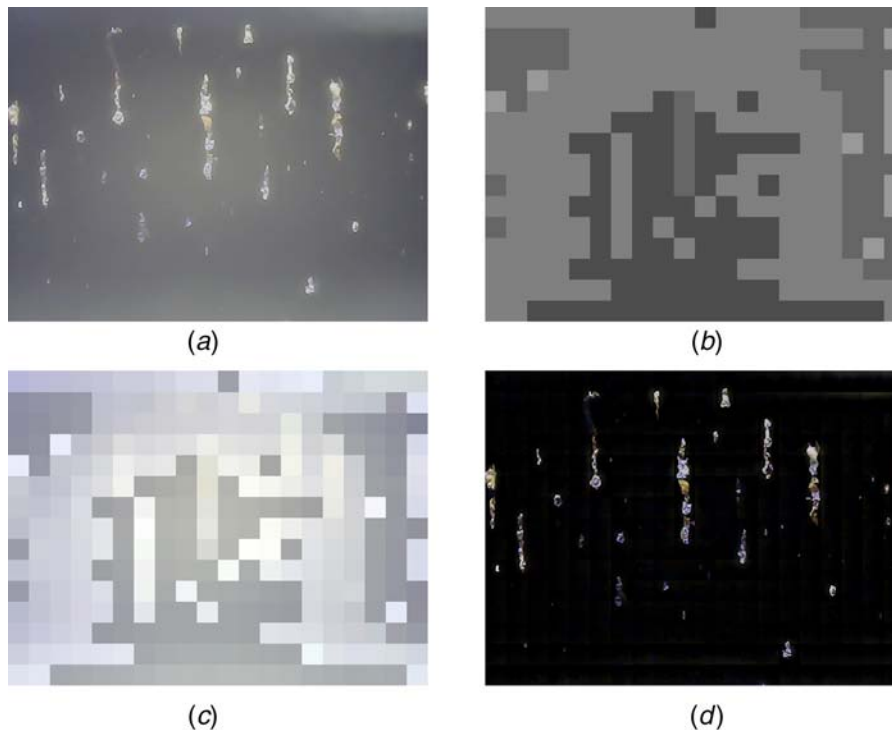


Fig. 10 Restoration without refinement: (a) input image, (b) α image, (c) L image, and (d) resultant image

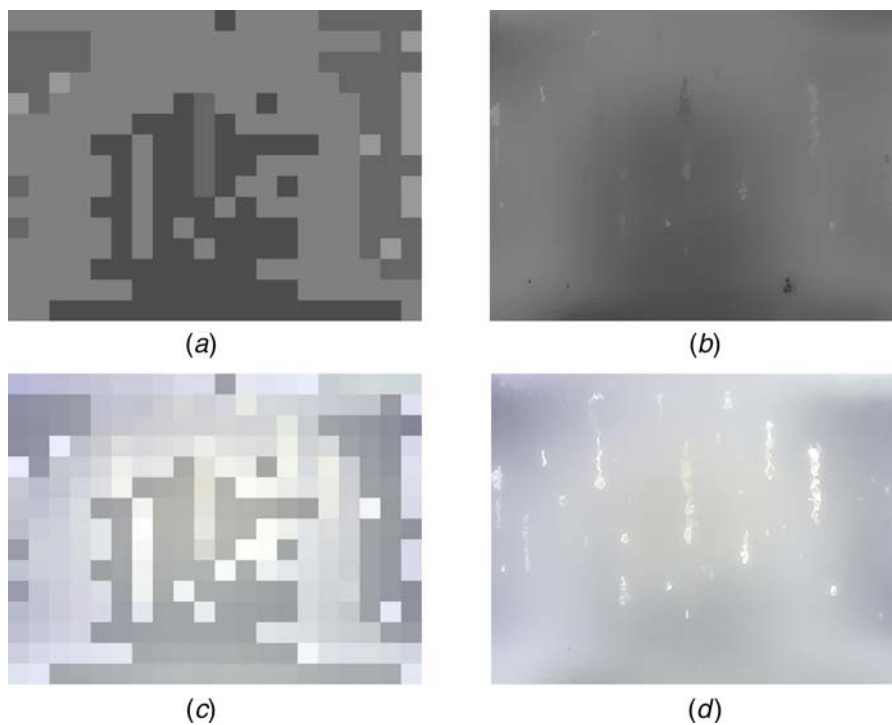


Fig. 11 Refinement results: (a) original α image, (b) refined α image, (c) original L image, and (d) refined L image

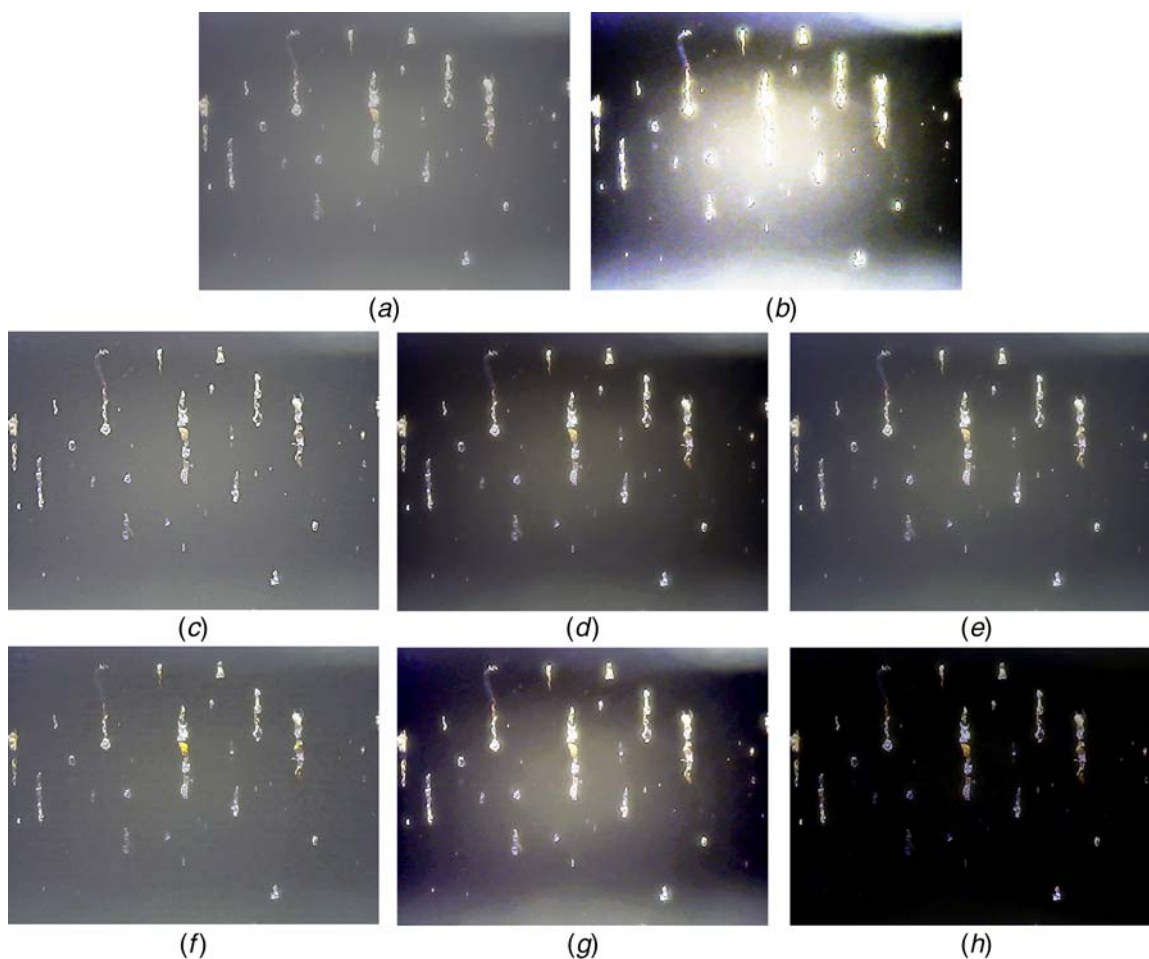


Fig. 12 Test image 1: (a) input, (b) HE, (c) UMF, (d) ACE, (e) DCPB method, (f) Fattal's method, (g) Kim's method, and (h) OCCE

included in the performance comparison. These include HE [15], UMF [16], ACE [18], dark channel prior-based method (DCPB method) [20], Fattal's method [21], and optimum contrast enhancement (Kim's method) [25]. Results are assessed qualitatively and quantitatively according to several widely used criteria.

4.1 Qualitative Evaluation. Two sample test images and their resultant images obtained from the proposed and related method are shown in Figs. 12 and 13. The qualitative evaluation is conducted by visually comparing the degree of scattering light removal, artifacts, and wear debris appearance.

It can be observed that input images, as shown in Figs. 12(a) and 13(a), have low contrast and saturation due to its undesirable capturing environment. Moreover, the wear debris pixels mostly have high intensity, and the color seems to be the same. From those images, it is difficult to identify wear debris accurately.

For scattering light and artifacts, the HE method produces obvious artifacts and leads to nonuniform illumination enhancement. Most wear debris are covered with the enhanced scattered light, and no effective information can be obtained from the images in Figs. 12(b) and 13(b). The similar drawback can be found in the Kim's method due to contrast enhancement in both background and foreground as shown in Figs. 12(g) and 13(g).

For the wear debris appearance, UMF only enhances the wear debris edges seen in Figs. 12(c) and 13(c), while color cast still exiting. Although ACE shows a good performance in color

correction in Fig. 12(d), it makes no difference to the second test image. Similarly, Fattal's method works well in Fig. 12(f), but results in poor appearance in Fig. 13(f). It proves that assumption-based methods cannot be directly applied to ferrography images restoration. In addition, DCPB method does not work for the situation shown in Fig. 13(e) due to large bright wear debris, and the restored color is inaccurate.

For the proposed method, results are shown in Figs. 12(h) and 13(h). On the one hand, the scattered light covering over the image is removed, and the original image is obtained. Furthermore, wear debris with different colors, such as blue and tawny wear debris, can be easily identified in the resultant images. Compared with other methods, the proposed method performs more satisfactorily and robustly.

4.2 Quantitative Evaluation. Criteria including colorfulness, average saturation, and contrast are calculated and displayed in the box plots as shown in Fig. 14. The mean and median values are included as annotations above the plots, and the mean values are summarized in Table 1 for comparison. Since wear debris appearance is the focus, only foreground pixels are considered in these statistics. Colorfulness is given by Eq. (3). ISD given by Eq. (10) is used to assess contrast. Average saturation is defined as follows:

$$S = \frac{1}{n} \sum_{i=1}^n \left(1 - \frac{3 \cdot \min \{r, g, b\}_i}{r_i + g_i + b_i} \right) \quad (35)$$

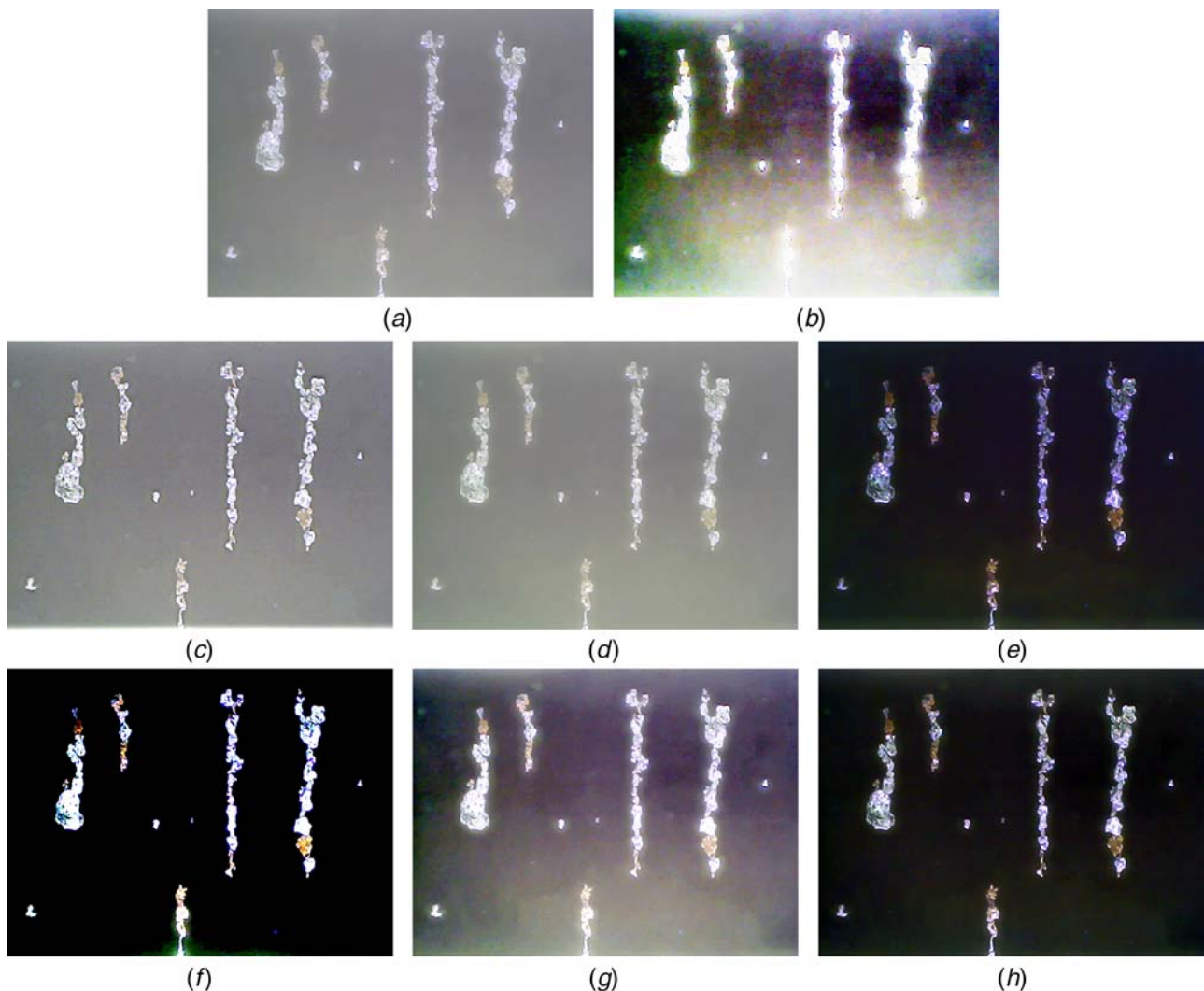


Fig. 13 Test image 2: (a) input, (b) HE, (c) UMF, (d) ACE, (e) DCPB method, (f) Fattal's method, (g) Kim's method, and (h) OCCE

Table 1 The results for each method mean values

Criteria	Input	HE	UMF	ACE	DCPB	Fattal	Kim	OCCE
Colorfulness	0.065	0.063	0.087	0.066	0.109	0.218	0.096	0.152
ISD	0.198	0.224	0.246	0.221	0.248	0.342	0.249	0.250
Saturation	0.036	0.017	0.041	0.010	0.062	0.137	0.053	0.146

For colorfulness, results of the proposed method have a mean value of 0.152, which is higher than those of other methods expect for the Fattal's method (0.218). This is the same with contrast evaluation. Results of the proposed method at 0.250, ranking the second high mean value. However, it can be found that over enhancements, shown in Figs. 12(f) and 13(f), make the two metrics resulting in a high level. In addition, the average saturation shows a sharp increase from 0.036 in input to 0.146 in the proposed method. Mean values of all other methods are lower than that of the proposed method.

As discussed earlier, the restored image quality are expected to be improved to the level of offline ferrography image in both color and contrast. From Figs. 14(a) and 14(b), the mean value of colorfulness after proposed restoration is a bit higher than 0.143 as shown in Fig. 6(a), and the restored contrast is close to 0.274 as shown in Fig. 7(b).

5 Conclusions

Aiming at recovering wear debris information, a method based on optimum color and contrast enhancement is developed for online ferrography image restoration. By analyzing the image capturing process, a degradation model is first constructed. Images are divided into blocks to reduce the difficulty to obtain undetermined parameters in the model. With the purpose of improving the image quality in both color and contrast, cost functions based on priors are formulated. Optimal parameters in each block are obtained by minimizing the cost functions using Lagrange multiplier, and these parameters are further refined into pixel-wise by guided filtering before restoration. Experimental results show that the proposed method is capable of removing the influence of the scattered light. With the wear debris appearance restored, colorfulness and contrast are improved to the level of of-line ferrography images, which facilitates subsequent processing including object extraction, identification, and classification.

Acknowledgment

This work was supported in part by National Key R&D Program of China (Grant No. 2018YFB1306100), in part by the National Natural Science Foundation of China (Funder ID: 10.13039/501100001809) (No. 51675403), in part by the International Collaborative Plan of Shaanxi Province (No. 2017kw-034), and in part by HPC Platform, Xi'an Jiaotong University (Funder ID: 10.13039/501100002412). Meanwhile, the authors gratefully acknowledge the support of K.C. Wong Education Foundation (Funder ID: 10.13039/501100012692).

References

- [1] Kumar, M., Shankar Mukherjee, P., and Mohan Misra, N., 2013, "Advancement and Current Status of Wear Debris Analysis for Machine Condition Monitoring: A Review," *Ind. Lubr. Tribol.*, **65**(1), pp. 3–11.
- [2] Dempsey, P. J., and Afjeh, A. A., 2004, "Integrating Oil Debris and Vibration Gear Damage Detection Technologies Using Fuzzy Logic," *J. Am. Helicopter Soc.*, **49**(2), pp. 109–116.
- [3] Higgs, P. A., Parkin, R., Jackson, M., Al-Habaibeh, A., Zorriassatine, F., and Coy, J., 2004, "A Survey on Condition Monitoring Systems in Industry," ASME 7th Biennial Conference on Engineering Systems Design and Analysis, Manchester, UK, July 19–22, American Society of Mechanical Engineers, pp. 163–178.
- [4] Akl, S. Y., El-Ghaffar, S. A., and Mosleh, H., 2016, "An Experimental Investigation of Industrial Gearbox Condition Using Wear Particle Analysis Technique," ASME 2016 International Mechanical Engineering Congress and Exposition, Phoenix, AZ, Nov. 11–17, American Society of Mechanical Engineers, p. V009T17A001.
- [5] Toms, A., Jordan, E., and Humphrey, G., 2005, "The Success of Filter Debris Analysis for J52 Engine Condition Based Maintenance," 41st AIAA/ASME/SAE/ASEE Joint Propulsion Conference & Exhibit, Tucson, AZ, July 10–13, p. 4338.
- [6] Roylance, B. J., 2005, "Ferrography—Then and Now," *Tribol. Int.*, **38**(10), pp. 857–862.
- [7] Du, L., and Zhe, J., 2011, "A High Throughput Inductive Pulse Sensor for Online Oil Debris Monitoring," *Tribol. Int.*, **44**(2), pp. 175–179.

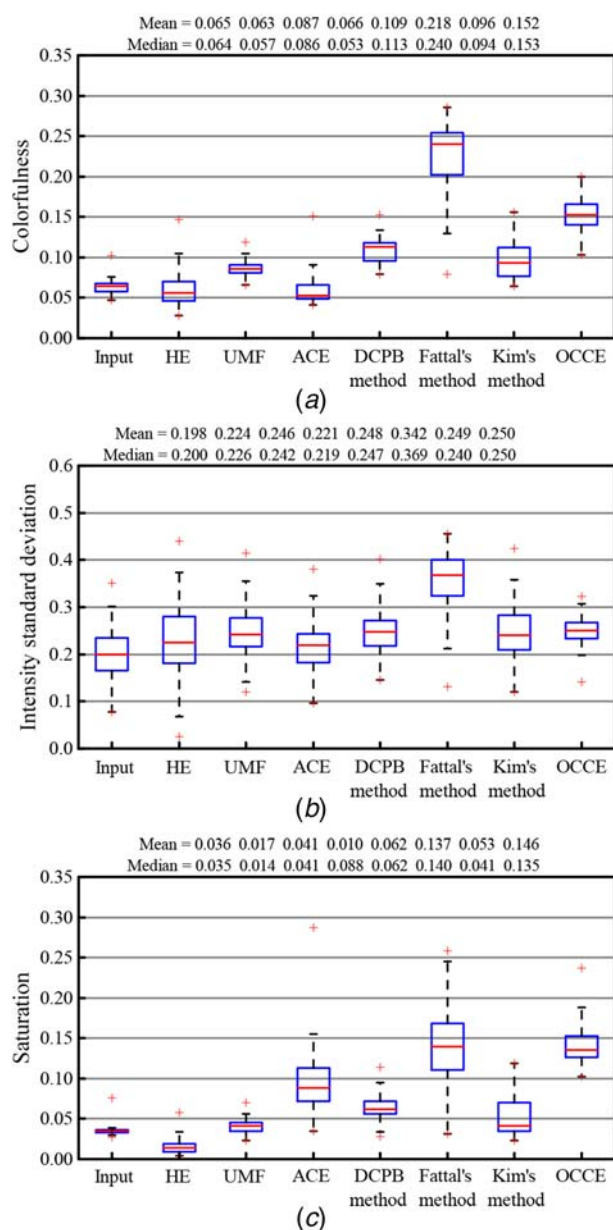


Fig. 14 Statistics of test results: (a) colorfulness, (b) intensity standard deviation, and (c) saturation

- [8] Wu, T. H., Mao, J. H., Wang, J. T., Wu, J. Y., and Xie, Y. B., 2009, "A New On-Line Visual Ferrograph," *Tribol. Trans.*, **52**(5), pp. 623–631.
- [9] Zhang, Y., Mao, J., and Xie, Y., 2011, "Engine Wear Monitoring With OLVF," *Tribol. Trans.*, **54**(2), pp. 201–207.
- [10] Wu, T., Peng, Y., Wu, H., Zhang, X., and Wang, J., 2014, "Full-Life Dynamic Identification of Wear State Based on On-Line Wear Debris Image Features," *Mech. Syst. Signal Process.*, **42**(1–2), pp. 404–414.
- [11] Wang, S., Wu, T., Wu, H., and Kwok, N., 2017, "Modeling Wear State Evolution Using Real-time Wear Debris Features," *Tribol. Trans.*, **60**(6), pp. 1022–1032.
- [12] Peng, Y., Wu, T., Wang, S., Kwok, N., and Peng, Z., 2015, "Motion-Blurred Particle Image Restoration for On-Line Wear Monitoring," *Sensors*, **15**(4), pp. 8173–8191.
- [13] Wu, H., Li, R., Kwok, N. M., Peng, Y., Wu, T., and Peng, Z., 2019, "Restoration of Low-Informative Image for Robust Debris Shape Measurement in On-Line Wear Debris Monitoring," *Mech. Syst. Signal Process.*, **114**(2019), pp. 539–555.
- [14] Xi, W., Wu, T., Yan, K., Yang, X., Jiang, X., and Kwok, N., 2018, "Restoration of Online Video Ferrography Images for Out-of-Focus Degradations," *EURASIP J. Image Video Process.*, **2018**(1), p. 31.
- [15] Kwok, N. M., Jia, X., Wang, D., Chen, S. Y., Fang, G., and Ha, Q. P., 2011, "Visual Impact Enhancement Via Image Histogram Smoothing and Continuous Intensity Relocation," *Comput. Electr. Eng.*, **37**(5), pp. 681–694.
- [16] Polesel, A., Ramponi, G., and Mathews, V. J., 2000, "Image Enhancement Via Adaptive Unsharp Masking," *IEEE Trans. Image Process.*, **9**(3), pp. 505–510.
- [17] Jmal, M., Soudene, W., and Attia, R., 2017, "Efficient Cultural Heritage Image Restoration With Nonuniform Illumination Enhancement," *J. Electron. Imaging*, **26**(1), p. 011020.
- [18] Rizzi, A., Gatta, C., and Marini, D., 2004, "From Retinex to Automatic Color Equalization: Issues in Developing a New Algorithm for Unsupervised Color Equalization," *J. Electron. Imaging*, **13**(1), pp. 75–85.
- [19] Getreuer, P., 2012, "Automatic Color Enhancement (ACE) and Its Fast Implementation," *Image Process. On Line*, **2**(2012), pp. 266–277.
- [20] He, K., Sun, J., and Tang, X., 2011, "Single Image Haze Removal Using Dark Channel Prior," *IEEE Trans. Pattern Anal. Mach. Intell.*, **33**(12), pp. 2341–2353.
- [21] Fattal, R., 2008, "Single Image Dehazing," *ACM Trans. Graphics (TOG)*, **27**(3), p. 72.
- [22] Zhu, Q., Mai, J., and Shao, L., 2015, "A Fast Single Image Haze Removal Algorithm Using Color Attenuation Prior," *IEEE Trans. Image Process.*, **24**(11), pp. 3522–3533.
- [23] Chiang, J. Y., and Chen, Y.-C., 2012, "Underwater Image Enhancement by Wavelength Compensation and Dehazing," *IEEE Trans. Image Process.*, **21**(4), pp. 1756–1769.
- [24] Tan, R. T., 2008, "Visibility in Bad Weather From a Single Image," 2008 IEEE Conference on Computer Vision and Pattern Recognition, Anchorage, AK, June 23–28, IEEE, pp. 1–8.
- [25] Kim, J. H., Jang, W. D., Sim, J. Y., and Kim, C. S., 2013, "Optimized Contrast Enhancement for Real-Time Image and Video Dehazing," *J. Visual Commun. Image Represent.*, **24**(3), pp. 410–425.
- [26] Nishino, K., Kratz, L., and Lombardi, S., 2012, "Bayesian Defogging," *Int. J. Comput. Vision*, **98**(3), pp. 263–278.
- [27] Wu, T., Wu, H., Du, Y., Kwok, N., and Peng, Z., 2014, "Imaged Wear Debris Separation for On-Line Monitoring Using Gray Level and Integrated Morphological Features," *Wear*, **316**(1–2), pp. 19–29.
- [28] Myshkin, N. K., Kong, H., Grigoriev, A. Y., and Yoon, E.-S., 2001, "The Use of Color in Wear Debris Analysis," *Wear*, **251**(1–12), pp. 1218–1226.
- [29] Hasler, D., and Suesstrunk, S. E., 2003, "Measuring Colorfulness in Natural Images," *Human Vision and Electronic Imaging VIII*, Vol. 5007, International Society for Optics and Photonics, Santa Clara, CA, June 17, pp. 87–96.
- [30] He, K., Sun, J., and Tang, X., 2013, "Guided Image Filtering," *IEEE Trans. Pattern Anal. Mach. Intell.*, **35**(6), pp. 1397–1409.